

An Integrated Region and Patch Feature Descriptor Model for Efficient Retrieval of Remote Sensing Images

Sudha S K^{1*}, Aji S²

^{1&2}Department of Computer Science,

University of Kerala, Thiruvananthapuram - 695581, Kerala, India

¹sudha.krishnaa@keralauniversity.ac.in

²aji@keralauniversity.ac.in

Article Info

Page Number: 111-123

Publication Issue:

Vol 71 No. 3s2 (2022)

Abstract

The region-based descriptors face difficulties representing the complex thematic classification of remote sensing images (RSI) with heterogeneous objects and backgrounds. The retrieval task using large archives thus becomes cumbersome on these images. Also, the region-based classification methods cannot consistently identify interest points on their boundaries. This work recommends a new object-based image retrieval framework incorporating a region and patch feature descriptor (RPFDF) for high-resolution remote sensing image retrieval (HR-RSIR) tasks. The method effectively combines local patch and region-based features into a region-based framework. The regional context features (RCF) are captured through an efficient seeded region growing segmentation (SRGSeg). The RCF integrates the augmented features from patches near the regions for better classification. The proposed integrated region and patch feature descriptor framework for RSIR (IRPFD-RSIR) focuses on reliable texture modeling at the region level, with an augmented patch-based feature descriptor to get more understanding of complex RSI. A weighted k-nearest neighbor (Wk-NN) classifier is incorporated for searching similar classes, utilizing an effective feature selection method. Three benchmark RSI datasets are used for evaluating the framework. The results compared with various feature descriptors and frameworks substantiate the overall efficiency of our retrieval model in terms of precision, recall, and F1-score.

Keywords: - Regional Context Feature, Remote Sensing Image Retrieval, Seeded Region Growing Segmentation, Patch-based Feature, Weighted k-Nearest Neighbor.

Article History

Article Received: 28 April 2022

Revised: 15 May 2022

Accepted: 20 June 2022

Publication: 21 July 2022

I. INTRODUCTION

With the advancements in high-resolution satellite sensor technology, a significant volume of research has been recently devoted to content-based remote sensing image retrieval (CB-RSIR) techniques. The volume of RSI archives is growing dramatically with advanced imaging sensors that can generate images with multiple resolutions and scales. Any successful RSIR model requires an automated, efficient data extraction and classification model to learn and retrieve the unstructured, complex RSI data. The large-scale RSI database requires reliable data infrastructure, efficient classification frameworks, and retrieval strategies. The complexity of massive RS data stems from the variety of different resolutions like spatial, spectral, and even temporal, which cause significant challenges to retrieval tasks. Hence, techniques that facilitate efficient search and retrieval

incorporating the image contents are to be formulated, which provides fast searching in very large RSI databases with minimal query specification.

The CB-RSIR systems follow a paradigm of representing the RSI with collected attributes, like color [1,2,3], texture [1,2,3,4], and shape [1,3,5,6]. Here, the retrieval is acquired by matching the feature set of the image query with those in the database. But, recent research in human perception of RSI content recommends the importance of semantic cues for efficient retrieval. The semantic gap between high-level perceptions and low-level features is overcome through incorporating relevance feedback mechanisms [1,7]. Also, the re-ranking and indexing techniques greatly intensify the retrieval performance by filtering out irrelevant classes [8,9,10,11].

Segmentation-based feature extraction has been popular in the RS domain [6], which generates a fine-grained representation of objects that embeds their spatial information. The segmentation procedure pulls out the significant objects-of-interest (OI) from the complex background of RSI. Several segmentation methods like region-based [12], watershed algorithms [13], threshold [14], and cluster-based [15] have been developed over the last decades. In practical applications, high-resolution RSI is challenging to automate for two reasons: i) their spatial resolution is higher, but their spectral resolution is lower, and ii) the surface texture features of small objects are not differentiable. These properties lead to maximized intra-class variability and minimized inter-class separability. Recent studies have proved that deeper networks could provide better solutions for object detection, visual recognition, and semantic segmentation tasks [16,17].

Object-based or region-based classification is popularizing in the RS domain [18, 19]. These methods intend to avoid the global description by representing images at the object level so that they can be close to the user's visual perception. The object-based framework offers the possibility of efficient computing of the textural features that characterize each class. The texture object provides added knowledge together with spectral data, which enhances the power to discriminate heterogeneous classes. However, the object/region-based methods cannot capture the features residing at the edges. Another popular approach for extracting the image content is by using patches. Patches are pre-determined shapes, like rectangles that are overlaid as a grid of specific size onto the irregular regions identified in the image. Recently, various patch-based techniques for high and very high resolution (VHR) multispectral image classification and indexing have been designed [20]. A patch-based approach is considered to combine deep features with the GEOBIA paradigm [21]. A combined patch-wise classification and hierarchical segmentation for multi-source RSI is proposed [22].

Motivated by this fact, in this proposed work, a new strategy for RSIR is recommended to retrieve similar images from large RSI repositories utilizing an integrated region and patch feature descriptor (IRPFD) framework. A seeded region growing (SRGSeg) segmentation technique is incorporated for generating homogeneous texture regions of the RSI. But no regular textures exist in many complex RSIs that discriminate between the object class and the background. In this view, the descriptors defined on pre-determined pixel supports or patches can provide additional internal details, which will enhance reliable classification. It is known that the patch-based descriptors can detect and encode the non-repetitive features and their spatial extension in a reliable manner [23]. The significant contribution of the recommended work is the infusion of local-patch-based features augmented into a region-based framework utilizing the regional context features (RCF). An efficient weighted k-nearest neighbor (Wk-NN) classifier performs a nearest neighbor retrieval. The contributions of the proposed IRPFD-RSIR method are outlined as follows.

i) A novel integrated region-patch feature descriptor (IRCFD) is derived for object localization-based efficient RSIR framework.

ii) The IRCFD efficiently captures the feature patterns from the complex RSI from the regions segmented through a seeded region growing segmentation technique for classification.

iii) The retrieval incorporates a likelihood-based feature selection, making the classifier efficient in learning from large RSI archives.

iv) The IRPFD-RSIR method remains bounded by the region-based framework with the leverage of additional features detected through patches, incorporating location and scale information, and achieved better performance using Wk-NN.

Many reviews are presented in literature by many researchers with respect to ML and IoT in different domain.[31][32][33][34]. This analysis will surely enable the researchers with the idea of ML technique in different applications. [35-39].The remaining part of the work is structured as follows. In Section 2, we detail the proposed IRPFD-RSIR approach for high-resolution RSI. Section 3 describes the experiments and results, and Section 4 concludes the work.

II. PROPOSED METHODOLOGY

The RSI has complex and diverse backgrounds that are not essential in identifying them for a respective class. Hence the IRPFD-RSIR method begins with a seeded region growing segmentation phase, which divides the input RSI into semantically meaningful homogeneous texture regions. The second phase is the extraction of the RCF from the segmented regions. The texture feature descriptors (TFD) and RCF vocabularies facilitate discrimination among different object classes from its background. Wk-NN evaluates each feature's discriminative score. The IRPFD-RSIR finds similar images and local regions for matching a query, irrespective of complex background. The overall representation of the IRPFD-RSIR method is shown in Figure 1.

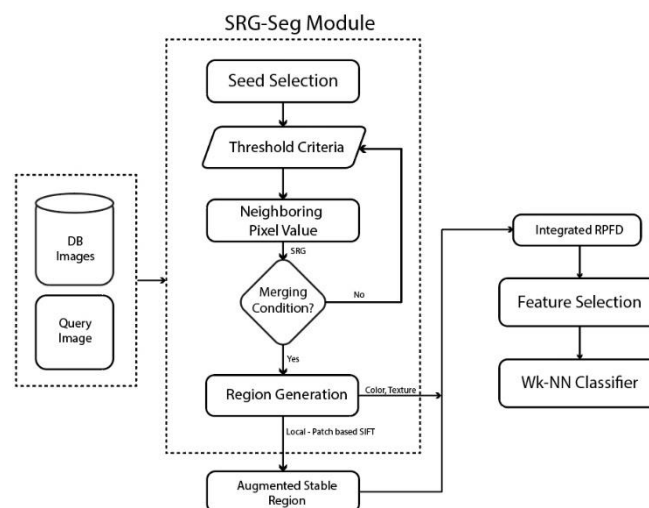


Fig. 1. Overall Representation of IRPFD-RSIR Framework

A. Seeded Region Growing Segmentation (SRGSeg)

Intra-class variation in RSI is often inhomogeneous due to scene characteristics, imaging environment, and image noise. Seeded region growing (SRGSeg) is a hybrid method that starts with assigned seeds and grows regions by merging a pixel to its nearest neighboring seeded region. SRGSeg is robust because of the characteristics of rapid and free-to-tune parameters. By performing

the seeded region growing algorithm, we intend to have spatially contiguous and homogenous pixels and different regions are with a high degree of heterogeneity. The SRGSeg consists of three major steps: seed selection, region growing, and region merging. The high-level knowledge of semantic image components can be leveraged by picking the appropriate seeds for growing more meaningful regions, which is an advantage of SRGSeg.

In the SRGSeg method, the initial seed selection is crucial because it decides the overall segmentation performance. An automatic seed selection criterion is chosen with some pre-defined conditions.

- i) The seed point candidate is ensured not to be residing on the boundary of two regions.
- ii) The candidate seed point should be inside the selected ROI with the highest similarity between its neighbors to represent the region accurately.
- iii) The distance from the seed pixel to its neighbors should be inside the extracted region to allow continuous growth.

For a given set of seeds, S_1, S_2, \dots, S_n each iteration of SRGSeg involves one additional pixel to one of the seed sets and is then replaced by the centroids of generated homogeneous regions, R_1, R_2, \dots, R_n by incorporating the added pixels step by step. The pixels from the same region are labeled, and the others are unlabeled pixels. Let H be the set of unlabeled pixels adjacent to at least one of the labeled regions.

$$H = \{(x, y) \notin \bigcup_{i=1}^n R_i | N(x, y) \cap \bigcup_{i=1}^n R_i \neq \emptyset\} \quad (1)$$

where $N(x, y)$ is the second order neighborhood of the pixel (x, y) . For the unlabeled pixel $(x, y) \in H$, $N(x, y)$ meets one of the labeled image regions R_i and define $\varphi(x, y) \in \{1, 2, \dots, n\}$ to be that index such that $N(x, y) \cap R_{\varphi(x, y)} \neq \emptyset$. The difference between the testing pixel at (x, y) and its adjacent labeled region R_i is defined as $\delta(x, y, R_i)$ and calculated as:

$$\delta(x, y, R_i) = |g(x, y) - g(X_i^c, Y_i^c)| \quad (2)$$

where $g(x, y)$ represents the values of the color components of the testing pixel (x, y) . $g(X_i^c, Y_i^c)$ represents the average values of three color components of the homogeneous region R_i , with the centroid (X_i^c, Y_i^c) . If $N(x, y)$ meets two or more labeled regions, $\varphi(x, y)$ takes a value of i such that $N(x, y)$ meets R_i and $\delta(x, y, R_i)$ is minimized as:

$$\varphi(x, y) = \min_{(x, y) \in H} \{\delta(x, y, R_j) | j \in \{1, 2, \dots, n\}\} \quad (3)$$

SRGSeg procedure for each boundary pixel will stop if the boundary pixels for the neighboring regions are connected or the color similarity distance is above an optimal threshold value. The stopping criterion of region growing is the choice of an optimal threshold value, which maintains the contour of the identified object regions. The threshold value kept being higher enough to extract the whole region from the entire scene image. The SRGSeg grows regions by recursively including similar neighboring and connected pixels to the seed pixel. The objective function aims to measure the quality of the resulting segmentation concerning maximized intra-segment homogeneity and inter-segment heterogeneity. The intersegment heterogeneity is measured using the Moran's I

autocorrelation index (MAI) [24]. It measures the degree of spatial correlation as reflected in the dataset altogether.

$$\text{MAI} = \frac{n \sum_{i=1}^n \sum_{j=1}^n w_{ij} (y_i - \bar{y})(y_j - \bar{y})}{(\sum_{i=1}^n (y_i - \bar{y})^2) (\sum_{i \neq j} \sum w_{ij})} \quad (4)$$

MAI is measured for the total number of regions, with spatial proximity w_{ij} for the mean color value of the region and the image. If regions R_i and R_j are adjacent, the value of w_{ij} is equal to one, otherwise zero. Two criteria are considered: the color similarity and the region size. The color features are determined using the L*u*v* color space for the texture feature extraction. The SRGSeg extracts the regions irrespective of their rotation, scale, or spatial relations to bring about a possible object region without low-level spatial information. Each region generated is expressed as a texture portion once it has been segmented concerning a particular scale. Then, K-means clustering is applied on the TFD for all the input images at all three scales to derive a vocabulary of texture words $T = \{T_i\}_{i=1}^{NT}$ and assign the respective regions to their nearest texture word.

B. Regional Context Features (RCF) Generation

A model that represents the relationships among each region and its neighborhood is to be established from the segmented regions. Even though the regions are comprised of a homogeneous group of pixels in color-texture space, their size and shape are not repeated across the instances of similar classes. Two regions are optimally separated using patches as local descriptors to generate a potential discriminative score. Patches are created by partitioning the object region into $N \times N$ grids. The grid size is adaptively defined based on the boundary area of the regions. Only those patches covering the region boundary are used for the feature extraction. Each patch covers an internal and external region, and the patches in which any of these regions have an area more than 15% of the patch area are considered.

The 128-D SIFT extraction [25] is incorporated for the local-descriptors $\{d_i\}$, for points, $P = \{P_i\}_{i=1}^{NP}$, with scale values, $\{\sigma_i\}$ to define proximity to regions. By clustering the descriptors from the training samples, a vocabulary of local-descriptor words of size N_W is formed. Let w_i be the nearest word to the descriptor d_i ; for each region of the local words that is at most $k\sigma_i$ pixels away, a histogram is constructed. The histograms are then appended and weighted inversely proportional to their k values to generate regional context Histograms (RCH).

Histograms are constructed for a generated region R with its member pixels, $\{r_j\}_{j=1}^{NR}$, with h_k be the k^{th} histogram for that region with N_W bins. K-means clustering is applied on the RCH for all training samples for all the image scales for constructing the vocabularies. The RCF is the cluster center, with regions assigned to the RCF nearest to their RCH. The TFD and RCF vocabularies discriminate between the object class and the RSI background. The TFDs and RCFs are combined into an integrated feature vector and used for learning with positive and negative regions. Here, any relevant feature, possibly lost or diminished in the region-based representation, will be reinforced by introducing the local patch-based descriptors.

C. Feature Selection

In order to effectively reduce the complexity of performing the nearest neighbor search on the IRPFD, the discriminative feature score (DFS) for each feature has been evaluated using a feature selection technique based on the likelihood ratio where the images are labeled as positive object class or negative. The discriminative score of the feature F_i is given as:

$$\tilde{R}(F_i) = \frac{P(F_i|O)}{P(F_i|O)+P(F_i|\bar{O})} \quad (5)$$

Where $P(F_i|O)$, is the conditional probability of a descriptor from an object image to be assigned to a specific feature cluster i and $P(F_i|\bar{O})$ is the non-object images. The features are ranked similarly to the likelihood ratio by the score.

$$R(F_i) = \frac{P(F_i|O)}{P(F_i|\bar{O})} \quad (6)$$

The descriptors of the image with a high probability give a strong indication of the presence of an object, which enhances the performance of the classifier framework used.

D. Weighted k-Nearest Neighbor Classification

The conventional KNN is computationally expensive as it searches the nearest neighbors for the new point at the prediction stage. When the K value is high, it is sensitive to outliers. The KNN method can be adapted in high-dimensional RSI classification for fast-finding the nearest samples with reduced complexity by using the highly discriminative feature samples selected based on the likelihood. Hence, the overall performance of the weighted k-nearest neighbor (Wk-NN) classifier is improved with less complexity.

The Wk-NN classification algorithm has received increased attention recently. The insight behind Wk-NN is to give more weight to the nearby points and less weight to the farther away points. Let $L = \{(x_i, y_i)\}_{i=1}^N$, be the training set of observations x_i with a given class label y_i and let x' be a new query point whose class label y' has to be predicted. The Wk-NN measures the distance between the query point and every other point in the training set. Then a set L' of k -nearest training data points to the query points are selected. The set $L' = \{(x_i^{NN}, y_i^{NN})\}_{i=1}^k$ is arranged in increasing order in terms of Euclidean distance. The closest neighbors are weighted more than the farther ones, using the distance-weighted function. The classification prediction of the query point is made by the majority weighted voting as in (7).

$$y' = \underset{y}{\operatorname{argmax}} \sum_{(x_i^{NN}, y_i^{NN}) \in L'} w_i \times \delta(y = y_i^{NN}) \quad (7)$$

where,

$$w_i = \begin{cases} \frac{d(x', x_k^{NN}) - d(x', x_i^{NN})}{d(x', x_k^{NN}) - d(x', x_1^{NN})}, & \text{if } d(x', x_k^{NN}) \neq d(x', x_1^{NN}) \\ 1, & \text{if } d(x', x_k^{NN}) = d(x', x_1^{NN}) \end{cases}$$

(8)

The Dirac delta function $\delta(y = y_i^{NN})$ takes a value of one if $(y = y_i^{NN})$ and zero otherwise. The overall classification performance is considering the k-nearest neighbors; hence an optimum value of

K or the number of nearest neighbors is to be determined. The optimal K value and the ranking of discriminative feature scores improve the voting by reducing the impact of irrelevant features.

III. EXPERIMENTAL RESULTS

This section reports the results obtained for the proposed IRPFD-RSIR framework on three benchmark RSI datasets with a comparative analysis with few other available methods. The total performance of the model has been validated using different metrics.

A. RSI Datasets and Validation Protocols

Three benchmark RSI datasets, the UCMD [26], RS-19 [27], and SIRI-WHU [28], are utilized for evaluating the overall efficiency of the IRPFD-RSIR framework. The UCMD contains 21 Land-Use/Land-Cover (LULC) categories of HR Aerial images. Each class contains 100 image samples with a pixel resolution of 0.3 m. and size 256×256 . The RS-19 dataset contains 19 classes of satellite scenes with 50 RGB images having size 600×600 . The SIRI-WHU contains 12 classes of HR satellite images gathered from the Google Earth imagery. Each class has about 200 RGB images of size 200×200 with a spatial resolution of 2 m. All the datasets are challenging with overlapping classes and complex backgrounds. The test-train split selected are i) UCMD – 80/20; ii) RS-19 – 60/40 and iii) SIRI-WHU – 50/50, respectively. The proposed model's retrieval performance is evaluated using the precision (P), recall (R), and F1-Score.

$$\text{Precision} = \frac{TP}{TP+FP} \quad (9)$$

$$\text{Recall} = \frac{TP}{TP+FN} \quad (10)$$

where TP is the number of true positive values, FP is the number of false-positive values, and FN is the number of false negatives. F1-Score is the weighted average of P and R and takes both false positives and false negatives into account.

$$F1 = \frac{2 \times \text{Precision} \times \text{Recall}}{\text{Precision} + \text{Recall}} \quad (11)$$

The performance evaluations conducted for the proposed retrieval method are detailed in the following sections.

B. Impact of K value on Wk-NN

The selection of the neighborhood size K has a consequential impact on the overall performance of the Wk-NN. Results considering different values for K are performed in all three datasets, and the respective accuracy values obtained for the values from 5 to 14 are plotted in Figure 2.

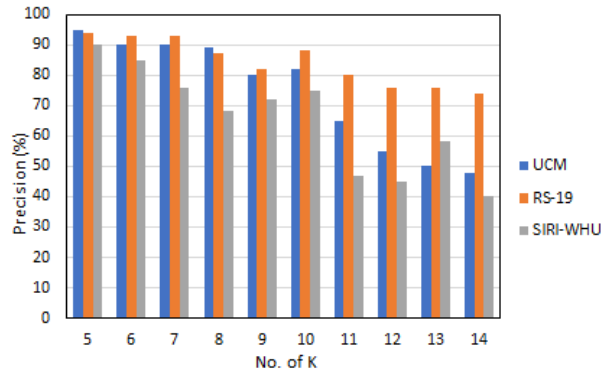


Fig. 2. Precision values obtained for different values for K

We got a reasonable precision value from 94% to 90% for the K values 5 to 10 with minimum validation errors. While choosing K values 11 to 14, the UCMD and SIRI-WHU datasets show significantly less accuracy. The RS-19 shows better accuracy than the other two datasets for all the K values. A degradation of precision for some classes in SIRI-WHU is noted due to the high overlapping nature, which is reflected in the total performance of the model. Also, some classes are influenced by the size and number of patches utilized to extract the local descriptors.

C. Evaluating Retrieval Performance

The overall performance of the IRPFD-RSIR framework achieved a better response in P, R, and F1 for all three datasets. Better precision values for the combined region-patch feature descriptor for all RSI datasets are observed than using the single feature descriptors. We compared the proposed IRPF descriptors for RSIR with other descriptors extracted for evaluation—the comparative measures given in Table 1 are for the precision for P@K=5.

TABLE I. COMPARATIVE ANALYSIS OF VARIOUS FEATURE DESCRIPTORS USED

Method	UCMD	RS-19	SIRI-WHU
Texture (Alone)	81.02 %	87.3 %	76.49 %
RCF (Alone)	74.29 %	80.16 %	73.88 %
Texture + RCF (IRPFD)	95.23 %	94.11 %	90.31 %

Most of the classes from the three datasets achieved better retrieval accuracies. The average precision, recall, and F1 scores obtained for the three RSI datasets are plotted in Table 2.

TABLE II. PRECISION, RECALL & F1-SCORE OBTAINED FOR ALL DATASETS

Dataset	Precision	Recall	F1-Score
UCMD	0.95	0.91	0.93
RS-19	0.94	0.93	0.93

SIRI-WHU	0.90	0.86	0.88
----------	------	------	------

Figures 3 (a) and 3 (b) represent the average precision of each retrieval after each iteration with $K = 5$ and $K = 10$, respectively. The proposed IRPFD-RSIR framework achieved the highest accuracy using the UCMD, RS-19, and SIRI-WHU datasets for the $K = 5$ compared to $K = 10$.

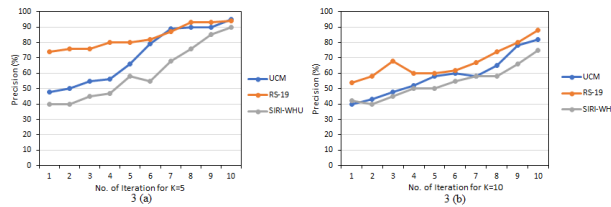


Fig. 3 (a). Precision for $K=5$ & 3 (b). Precision for $K=10$

The W_k -NN is highly responsive to the selection of K value, and it generates different accuracy measures with the respective choice of K . For a too small K value, the model becomes sensitive to outliers, and for a large K value, the neighborhood includes too many points from other classes. Hence a reasonable value has been chosen from $K = 5$ to $K = 14$, for which the model achieved a good precision metric for $K = 5$. The clustered DFS reduced the influence of the sensitivity of the selection of K to some degree and achieved better performance.

D. Comparison with other Methods

We compared the IRPFD-RSIR framework with a few methods, those incorporating classical methods for evaluation. We did not consider the methods implemented using deep learning architectures, which are computationally complex and expensive, with higher precision rates when compared to the conventional methods. Table 3 shows the comparative measures for the average precision obtained using the UCMD dataset.

TABLE III. COMPARATIVE ANALYSIS WITH OTHER METHODS

Method	Average Precision
Ensemble-Color [29]	0.65
Ensemble-Texture [29]	0.83
Ensemble All [29]	0.86
Multi-Color [29]	0.57
Multi-Texture [29]	0.74
Multi All [29]	0.75
Circular Relevance Feedback-BoW [30]	0.83
W_k -NN-TFD (Ours)	0.81
W_k -NN-RCF (Ours)	0.74
W_k-NN-IRPFD (Proposed)	0.95

The proposed IRPFD-RSIR model showed statistically significant performance over the frameworks compared. The combined efficiencies of both the regional as well as patch-based feature descriptors are successful in providing better performance. The Wk-NN classifier efficiently searches for the nearest neighbors using the clustered discriminative features scores of the IRPFD. Also, the weight computing decision rule overcomes the influence of the sensitivity and enhances the classification performance of Wk-NN.

IV. CONCLUSION

We proposed an efficient RSIR framework using a combined region-patch feature descriptor. Using a patch-based approach bounded by a region-based framework, we aim to extract descriptors that capture both spectral and structural information for better retrieval results. The proposed IRPFD-RSIR performs object-based classification and localization within a region-based framework incorporating both texture feature descriptors and regional context features. The highly complex objects with repetitive patterns can be modeled using the texture and spatial information into an encapsulated regional context feature. The Wk-NN classifier for the proposed IRPFD-RSIR framework achieves better precision, recall, and F1-Score for the three RSI datasets. Different K values are validated for all datasets, and it is evident that the K value 5 obtained the highest precision. The average precision values obtained for the UCMD, RS-19, and SIRI-WHU datasets are; 95.23 %, 94.11 %, and 90.31 %, respectively. The results proved that:

- The integrated region-patch feature descriptor efficiently captures the essential feature representations from the complex RSI datasets.
- The IRPFD-RSIR method is bounded by a region-based framework taking favor of the supportive features generated through the patches, along with location and scale information.
- The high DFS likelihood improved the performance of the Wk-NN retrieval model.

REFERENCES

1. Ferecatu, M., and Boujemaa, N., "Interactive remote sensing image retrieval using active relevance-feedback," *IEEE Tr. on Geoscience and Remote Sensing*, (2007); 45(4), 818–826.
2. Ma, C.; Dai, Q.; Liu, J.; Liu, S. and Yang, J., "An improved SVM model for relevance-feedback in remote sensing image retrieval," *International Journal of Digital Earth*, (2014); 7(9), 725–745.
3. Wang, M.; and Song, T., "Remote sensing image retrieval by scene-semantic matching," *IEEE Tr. on Geoscience and Remote Sensing*, (2013); 51(5), 2874–2886.
4. Aptoula, E., "Remote sensing image retrieval with global-morphological texture descriptors," *IEEE Tr. on Geoscience and Remote Sensing*, (2014); 52(5), 3023–3034.
5. G. Scott, M. Klaric, C. Davis and C.-R. Shyu, "Entropy balanced bitmap tree for shape-based object retrieval from large-scale satellite imagery databases," *IEEE Tr. on Geoscience and Remote Sensing*, (2011); 49(5), 1603– 1616.
6. Chaudhuri, B.; Demir, B.; Bruzzone, L.; and Chaudhuri, S., "Region-based retrieval of remote sensing images using an unsupervised graph-theoretic approach," *IEEE Geoscience and Remote Sensing Letters*, (2016); 13(7), 987–991.
7. Demir, B. and Bruzzone, L., "A novel active-learning method in relevance-feedback for content-based remote sensing image retrieval," *IEEE Tr. on Geoscience and Remote Sensing*, (2014); 53(5), 2323–2334.
8. Tang, X.; and Jiao, L., "Fusion similarity-based re-ranking for SAR image retrieval. *IEEE Geoscience and Remote Sensing Letters*," (2017); 14(2), 242–246.

9. Wang, Y.; Zhang, L.; Tong, X.; Zhang, Z.; Liu, H.; et al., "A three-layered graph-based learning approach for remote sensing image retrieval," *IEEE Tr. on Geoscience and Remote Sensing*, (2016); 54(10), 6020–6034.
10. Bin Luo, Shujing Jiang, and Liangpei Zhang, "Indexing of remote sensing images with different resolutions by multiple features," *IEEE Journal of Selected Topics in Applied Earth Observations and Remote Sensing*, (2013); 6(4), 1899-1912.
11. Shijin LI, Hui YU, and Lixin YUAN, "A novel approach to remote sensing image retrieval with multi-feature, VP-tree indexing, and online feature selection," *Proceedings - 2016 IEEE 2nd International Conference on Multimedia Big Data, BigMM*, (2016); 133-136.
12. L. Hashemi-Beni and A. A. Gebrehiwot, "Flood extent mapping: An integrated method using deep learning and region growing using UAV optical data," *IEEE Journal of Selected Topics in Applied Earth Observation and Remote Sensing*, (2021); 14, 2127–2135.
13. H. Huang, X. Li, and C. Chen, "Individual tree-crown detection and delineation from very-high-resolution UAV images based on bias field and marker-controlled watershed segmentation algorithms," *IEEE Journal of Selected Topics in Applied Earth Observation and Remote Sensing*, (2018); 11(7), 2253–2262.
14. CH. V. V. S. Srinivas, M. V. R. V. Prasad, and M. Sirisha, "Remote sensing image segmentation using OTSU algorithm," *International Journal of Computer Applications*, (2019); 178(12).
15. Raffaele Gaetano, Giuseppe Scarpa and Giovanni Poggi, "Hierarchical texture-based segmentation of multiresolution remote-sensing images," *IEEE Tr. on Geoscience and Remote Sensing*, (2009); 47(7).
16. S. Liu, C. He, H. Bai, Y. Zhang, and J. Cheng, "Light-weight attention semantic segmentation network for high-resolution remote sensing images," *In Proc. IEEE International Geoscience and Remote Sensing Symposium*, (2020); 2595–2598.
17. Yaning Yi, Zhijie Zhang, Wanchang Zhang, Chuanrong Zhang, Weidong Li, and Tian Zhao, "Semantic segmentation of urban buildings from VHR remote sensing imagery using a deep convolutional neural network," *MDPI, Remote Sensing*, (2019); 11, 1774; doi:10.3390/rs11151774.
18. Mohammad D. Hossain and Dongmei Chen, "Segmentation for object-based image analysis (OBIA): A review of algorithms and challenges from remote sensing perspective," *ISPRS Journal of Photogrammetry and Remote Sensing*, (2019); 150, 115-134, doi: 10.1016/j.isprsjprs.2019.02.009.
19. Vitor S. Martins, Amy L. Kaleita, Brian K. Gelder, Hilton L.F. da Silveira, and Camila A. Abe, "Exploring multi-scale object-based convolutional neural network (multi-OCNN) for remote sensing image classification at high spatial resolution," *ISPRS Journal of Photogrammetry and Remote Sensing*, (2020); 168, 56-73, doi: 10.1016/j.isprsjprs.2020.08.004.
- E. Georgescu, C. Vaduva, D. Raducanu and M. Datcu, "Feature extraction for patch-based classification of multispectral earth observation images," *IEEE Geoscience and Remote Sensing Letters*, (2016); 13(6), 865-869, doi: 10.1109/LGRS.2016.2551359.
20. Bo Liu, Shihong Du, Shouji Du, and Xiuyuan Zhang, "Incorporating deep features into GEOBIA paradigm for remote sensing imagery classification: A patch-based approach," *MDPI, Remote Sensing*, (2020); 12(18), 3007, doi:10.3390/rs12183007.

21. Xin-Yi Tong, Gui-Song Xia, Qikai Lu, Huanfeng Shen, Shengyang Li, Shucheng You, and Liangpei Zhang, "Land-cover Classification with High-Resolution Remote Sensing Images using Transferable Deep Models," *Remote Sensing of Environment*, (2020); 237, 1-35.
- D. Pantofaru, G. Dorko, C. Schmid, and M. Hebert, "Combining regions and patches for object class localization," *Conference on - Computer Vision and Pattern Recognition Workshop (CVPRW'06)*, (2006); 23-23, doi: 10.1109/CVPRW.2006.57.
22. Ghimire B., Rogan J., and Miller J., "Contextual land-cover classification: incorporating spatial dependence in land-cover classification models using random forests and the Getis statistic," *Remote Sensing Letters*, (2010); 1: 45-54. doi: 10.1080/01431 160903252327.
- E. G. Lowe, "Distinctive image features from scale-invariant keypoints," *IJCV*, (2004); 60(2):91–110.
23. Yang Y.; and Newsam S., "Bag-of-visual-words and spatial extensions for land-use classification," In *Proceedings: 18th Sigspatial International Conference on- Advances in Geographic Information Systems*, ACM, (2010); 270-279, doi:10.1145/1869790.1869829.
24. Dai, Dengxin, and Wen Yang, "Satellite image classification via. two-layer sparse coding with biased image representation," *IEEE Geoscience and Remote Sensing Letters*, (2011); 8(1), 173–176.
25. Zhao, B., Zhong, Y., Xia, G.S., and Zhang, L., "Dirichlet derived multiple topic scene classification model for high spatial resolution remote sensing imagery," *IEEE Transactions on Geoscience and Remote Sensing*, (2016); 54(4): 2108–2123, doi:10.1109/TGRS.2015.2496185.
26. Caihong Ma, Fu Chen, Jin Yang, Jianbo Liu, Wei Xia and Xinpeng Li, "A remote sensing image retrieval model based on an ensemble neural networks," *Big Earth Data*, (2018); 2(4), 351-367, doi:10.1080/20964471.2019.1570815.
27. X. Tang, X. Zhang, F. Liu and L. Jiao, "Circular relevance-feedback for remote sensing image retrieval," *IGARSS, IEEE - International Geoscience and Remote Sensing Symposium*, (2018); 8953-8956, doi: 10.1109/IGARSS.2018.8519393.
28. Ajitha, P.Sivasangari, A.Gomathi, R.M.Indira, K."Prediction of customer plan using churn analysis for telecom industry",*Recent Advances in Computer Science and Communications*, Volume 13, Issue 5, 2020, Pages 926-929.
29. "Sivasangari A, Ajitha P, Rajkumar and Poonguzhali," *Emotion recognition system for autism disordered people*", *Journal of Ambient Intelligence and Humanized Computing* (2019)."
30. Ajitha, P., Lavanya Chowdary, J., Joshika, K., Sivasangari, A., Gomathi, R.M., "Third Vision for Women Using Deep Learning Techniques", *4th International Conference on Computer, Communication and Signal Processing, ICCSP 2020*, 2020, 9315196
31. Sivasangari, A., Gomathi, R.M., Ajitha, P., Anandhi (2020), *Data fusion in smart transport using convolutional neural network*", *Journal of Green Engineering*, 2020, 10(10), pp. 8512–8523.
32. A Sivasangari, P Ajitha, RM Gomathi, "Light weight security scheme in wireless body area sensor network using logistic chaotic scheme", *International Journal of Networking and Virtual Organisations*, 22(4), PP.433-444, 2020
33. Sivasangari A, Bhowal S, Subhashini R "Secure encryption in wireless body sensor networks",*Advances in Intelligent Systems and Computing*, 2019, 814, pp. 679–686
34. Sindhu K, Subhashini R, Gowri S, Vimali JS, "A Women Safety Portable Hidden camera detector and jammer", *Proceedings of the 3rd International Conference on Communication and Electronics Systems, ICCES 2018*, 2018, pp. 1187–1189, 8724066.

35. Gowri, S., and J. Jabez. "Novel Methodology of Data Management in Ad Hoc Network Formulated Using Nanosensors for Detection of Industrial Pollutants." In *International Conference on Computational Intelligence, Communications, and Business Analytics*, pp. 206-216. Springer, Singapore, 2017.
36. Gowri, S. and Divya, G., 2015, February. Automation of garden tools monitored using mobile application. In *International Conference on Innovation Information in Computing Technologies* (pp. 1-6). IEEE.